

# NUMERICAL INVESTIGATION OF INVISCID HYPERSONIC FLOW OVER A REENTRY VEHICLE

**Heidi Korzenowski**

Universidade do Vale do Paraíba – São José dos Campos - SP  
heidi@univap.br

**Carlos Alberto Rocha Pimentel**

Universidade do Vale do Paraíba – São José dos Campos - SP  
cearapim@univap.br

**Abstract.** *The present work performs an inviscid hypersonic flow simulation over a re-entry body. A small ballistic re-entry vehicle SARA configuration is numerically investigated by using the Euler equations. The governing equations are discretized in conservative form in a cell centered, finite volume procedure for unstructured triangular grids. Spatial discretization considers the upwind scheme. A MUSCL reconstruction of primitive variables is used in order to determine left and right states at interfaces. Time march uses, an explicit 2nd-order accurate, 5-stage Runge-Kutta time stepping scheme. The Gardiner chemical kinetics considers 5 species with their combination and dissociation reactions. Mach number and pressure and temperature contours are presented. Ideal, inert and real gas will be considered. 79% of Nitrogen and 21% of Oxygen composes the gas. Freestream Mach 12 flow was selected to conduct numerical investigations.*

**Keywords.** *Hypersonic flow, reentry flow, finite volume.*

## 1. Introduction

The development of efficient numerical solvers is very important owing to the difficulties and high costs associated with the experimental work at high speed flows. Typical hypersonic flows undergo chemical and thermal processes that are very difficult to predict experimentally. Hence, the numerical simulation plays an important role in hypersonic vehicle design. The focus of the numerical methods is on the accurate simulation of flows with strong shock waves, capturing complex flow phenomena and variables variations for hypersonic flows (Anderson, 1989).

The hypersonic fluid flow simulation over a re-entry body is quite some interesting in sense that a strong detached normal shock wave in the nose region is generated. This phenomenon is particularly interesting because the curved bow shock is a normal shock wave in the nose region, and away from this one has all possible oblique shock solutions for a given freestream Mach number.

A finite volume formulation of compressible Euler equations in conservative form has been considered (Hirsh, 1990). A high-resolution scheme is employed in order to obtain a good spatially resolution of the flow features. In this work the simulations are performed by using a second-order Liu flux-vector splitting scheme (Liu, 1996), implemented in an unstructured grid context. This scheme considers a MUSCL approach, that is, the interface fluxes are formed using left and right states at the interface, which are linearly reconstructed by primitive variable extrapolation on each side of the interface (Azevedo and Korzenowski, 1998).

A minmod limiter is used in order to avoid any undesired oscillations in the solution. The equations are discretized in a cell centered based finite volume procedure on triangular meshes. Time march uses an explicit, second-order accurate, five-stage Runge-Kutta time stepping scheme.

For the gas flow simulations one considers that 79% of Nitrogen and 21% of Oxygen composes the gas. Real gas effects are considered for the reactive flow simulations (Pimentel, 2000). The chemical kinetic mechanism considers five chemical species, with their combination and dissociation reactions (Hachemin, 1995). The computations are performed considering  $M_\infty = 12$ . Results obtained for the inviscid simulations are presented, in order to analyse the phenomena presented in such flows. Results indicate that the scheme could adequately capture the flowfield features.

The simulations are concerned with the implementation of unstructured grid, mesh refinement techniques for two-dimensional inviscid flow problems of aerospace interest. The mesh refinement procedure uses a numerical sensor based on flow physical properties.

## 2. Mathematical model

The two-dimensional time-dependent, compressible Euler equation may be described, in conservative vector form, by

$$\frac{\partial Q}{\partial t} + \frac{\partial E}{\partial x} + \frac{\partial F}{\partial y} = 0. \quad (1)$$

The vectors E and F are conservative flux vectors, Q is the vector of conservative quantities. If the equations are discretized in a cell centered finite volume procedure, the discrete vector of conserved variables,  $Q_i$ , is defined as an

average over the  $i$ -th control volume. In this context, the flow variables can be assumed as attributed to the centroid of each cell. The Equation (1) can be written in integral form for the  $i$ -th control volume as

$$\frac{\partial}{\partial t}(V_i Q_i) + \int_S [E dy - F dx] = 0, \quad (2)$$

where  $V$  represents the area of the control volume and  $S$  its boundary.

The supersonic reactive flow will be computed using the unsteady 2-D Euler equations, thus neglecting molecular transport. These balance equations of mass, momentum, energy and species mass fraction can be written as

$$\frac{\partial Q}{\partial t} + \frac{\partial E}{\partial x} + \frac{\partial F}{\partial y} = \Omega, \quad (3)$$

where

$$Q = [\rho, \rho u, \rho v, \rho \varepsilon, \rho Y_1, \dots, \rho Y_{N-1}]^T, \quad E = \begin{bmatrix} \rho u \\ \rho u^2 + p \\ \rho uv \\ u(\rho \varepsilon + p) \\ \rho Y_1 u \\ \vdots \\ \rho Y_{N-1} u \end{bmatrix}, \quad F = \begin{bmatrix} \rho v \\ \rho uv \\ \rho v^2 + p \\ v(\rho \varepsilon + p) \\ \rho Y_1 v \\ \vdots \\ \rho Y_{N-1} v \end{bmatrix}, \quad (4)$$

considering

$$\Omega = [0, 0, 0, 0, \dot{\omega}_1 W_1, \dots, \dot{\omega}_{N-1} W_{N-1}]^T, \quad (5)$$

with  $p$ ,  $Y_N$  and  $\varepsilon$  given by

$$Y_N = 1 - \sum_{i=1}^{N-1} Y_i, \quad p = \rho R T \sum_{i=1}^N \frac{Y_i}{W_i}, \quad \varepsilon = \sum_{i=1}^N Y_i e_i + \frac{1}{2} (u^2 + v^2), \quad (6)$$

where

$$e_i = h_i^0 + \int_{T_0}^T c_{pi} dT - \frac{p}{\rho} \quad (7)$$

In these equations  $\varepsilon$  is the total energy per unit of mass,  $e$  is the internal energy,  $R$  is the universal gas constant. The internal energy, the standard-state enthalpy and the specific heat at constant pressure per unit of mass of species  $i$  are noted  $e_i$ ,  $h_i^0$  and  $c_{pi}$ .  $Y_i$  and  $W_i$  are the mass fraction and the molecular weight of chemical species  $i$ , respectively.

### 3. Chemical kinetics mechanism

The chemical kinetics mechanism for the reactive mixture of nitrogen and oxygen is due to Gardiner (Hachemin, 1995). This mechanism considers 5 species ( $N_2$ ,  $O_2$ ,  $N$ ,  $O$ ,  $ON$ ) and 21 elementary reactions, and is given in Table (1). The chemical production rates are given by the Arrhenius law,

$$k_f = A T^\beta \exp\left(\frac{-E_a}{T}\right). \quad (8)$$

Table 1. Reaction mechanism for  $N_2 - O_2$ :  $A$ (m, mol, s) e  $E_a$  (Kelvins)

Reações elementares	$A$	$\beta$	$E_a$ (Kelvins)
$N_2+N_2=>2N+N_2$	3.7e21	-1.6	113200.
$2N+N_2=>N_2+N_2$	1.08e13	-1.493	100.
$N_2+O_2=>2N+O_2$	1.4e21	-1.6	113200.
$2N+O_2=>N_2+O_2$	3.07e13	-1.493	100.
$N_2+NO=>2N+NO$	1.4e21	-1.6	113200.
$2N+NO=>N_2+NO$	3.07e13	-1.493	100.
$N_2+N=>2N+N$	1.6e22	-1.6	113200.
$2N+N=>N_2+N$	3.51e14	-1.493	100.
$N_2+O=>2N+O$	1.4e21	-1.6	113200.
$2N+O=>N_2+O$	3.07e13	-1.493	100.
$O_2+N_2=>2O+N_2$	3.64e18	-1.0	59380.
$2O+N_2=>O_2+N_2$	1.84e10	-0.714	109.
$O_2+O_2=>2O+O_2$	1.64e19	-1.0	59380.
$2O+O_2=>O_2+O_2$	8.28e10	-0.714	109.
$O_2+NO=>2O+NO$	1.82e18	-1.0	59380.
$2O+NO=>O_2+NO$	9.19e09	-0.714	109.
$O_2+N=>2O+N$	1.82e18	-1.0	59380.
$2O+N=>O_2+N$	9.19e09	-0.714	109.
$O_2+O=>2O+O$	4.56e19	-1.0	59380.
$2O+O=>O_2+O$	2.3e11	-0.714	109.
$NO+N_2=>N+O+N_2$	4.0e20	-1.5	75500.
$N+O+N_2=>NO+N_2$	2.16e19	-1.3217	97.
$NO+O_2=>N+O+O_2$	4.0e20	-1.5	75500.
$N+O+O_2=>NO+O_2$	2.16e19	-1.3217	97.
$NO+NO=>N+O+NO$	8.0e20	-1.5	75500.
$N+O+NO=>NO+NO$	4.32e19	-1.3217	97.
$NO+N=>N+O+N$	8.0e20	-1.5	75500.
$N+O+N=>NO+N$	4.32e19	-1.3217	97.
$NO+O=>N+O+O$	8.0e20	-1.5	75500.
$N+O+O=>NO+O$	4.32e19	-1.3217	97.
$N_2+O=>NO+N$	1.82e14	0.0	38370.
$NO+N=>N_2+O$	7.35e13	-0.07083	666.
$NO+O=>O_2+N$	3.8e09	1.0	20820.
$O_2+N=>NO+O$	4.07e10	0.886	4689.

The calculation of  $k_f$  and the molar production rates  $\dot{\omega}_k$  are performed using the CHEMKIN-II package. The thermodynamic properties are calculated according to the procedures developed by Kee et al (1991).

#### 4. Numerical technique

The numerical approach discretized the 2-D Euler equations in conservative form in an upwind, finite volume context considering an unstructured grid made up of triangles. The equations are discretized in a cell centered finite volume procedure. The spatial discretization algorithm is essentially concerned with finding a discrete approximation to the surface integral

$$C(Q_i) \cong \int_{S_i} (E dy - F dx) \quad (9)$$

For the flux-vector splitting case, a Liu formulation has been tested. The implementation of the 2nd-order scheme is based on an extension of the Godunov approach (Hirsh, 1990). The projection stage of the Godunov scheme, in which the solution is projected in each cell on piecewise constant states, is modified. This constitutes the so-called MUSCL approach for the extrapolation of primitive variables. By this approach, left and right states at a given interface are linearly reconstructed by primitive variable extrapolation on each side of the interface, together with some appropriate limiting process in order to avoid the generation of new extreme.

The numerical fluxes  $E$  and  $F$  can be expressed as the sum of the numerical convective flux and the numerical pressure flux at each cell interface (Liou, 1996). Therefore, the numerical convective flux is defined in terms of Mach

number, speed of sound and the quantity  $\Phi$ , defined as  $\Phi = (\rho, \rho u, \rho v, \rho H)^T$ . For the AUSM<sup>+</sup> formulation, the Mach number and the pressure are splitting accordingly some properties, as described in Liou (1996).

The Liou scheme implemented in this work considers that the convective operator can be expressed as a sum of the convective and pressure terms, given by the expression

$$C(Q_i) = (F_{ik}^{(c)} + P_{ik}) \ell_{ik}, \quad (10)$$

where  $\ell_{ik}$  represents the length of the  $ik$  edge. Expressions of the terms  $F_{ik}^{(c)}$  and  $P_{ik}$ , as well as details of the formulations can be found in Azevedo and Korzenowski (1998).

Even considering a 2<sup>nd</sup>-order flux vector splitting scheme with a MUSCL approach, it is possible to obtain oscillations in the solution. Therefore one must use nonlinear corrections, namely limiters, to avoid any oscillations. In this work a simple minmod limiter was adopted. Time integration used an explicit, 2nd-order accurate, hybrid method, which evolved from the consideration of Runge-Kutta time stepping scheme.

Adaptive mesh refinement, based on a sensor of flow property gradients, was performed to obtain a better resolution of strong discontinuities. The sensor definition could be expressed as

$$(\text{sensor})_i = \left\{ \max_n \left[ \frac{|\nabla \phi_n|}{|\phi_{n \max} - \phi_{n \min}|} \right] \right\}_i \quad (11)$$

where  $\phi_n \in (\rho, p, u, v, T)$ ,  $\phi_{n \max}$  and  $\phi_{n \min}$  are the maximum and the minimum values of the  $\phi_n$  property in the flowfield. All results presented in this work have used a sensor based on all primitive variables.

#### 4. Results

The small ballistic re-entry vehicle SARA configuration was used to perform the numerical simulations, assuming freestream Mach number 12. For the gas flow one considers 79% of Nitrogen and 21% of Oxygen composes the gas. Pressure and temperature initial conditions are 0.1847 atm and 300K, respectively.

The numerical simulations was obtained by using 2<sup>nd</sup>-order Liu flux vector splitting scheme. Although this scheme could capture strong discontinuities without smearing the solution, one observes the generation of spurious numerical oscillations behind the shock wave. The development of the carbuncle is visible in Figure (1).

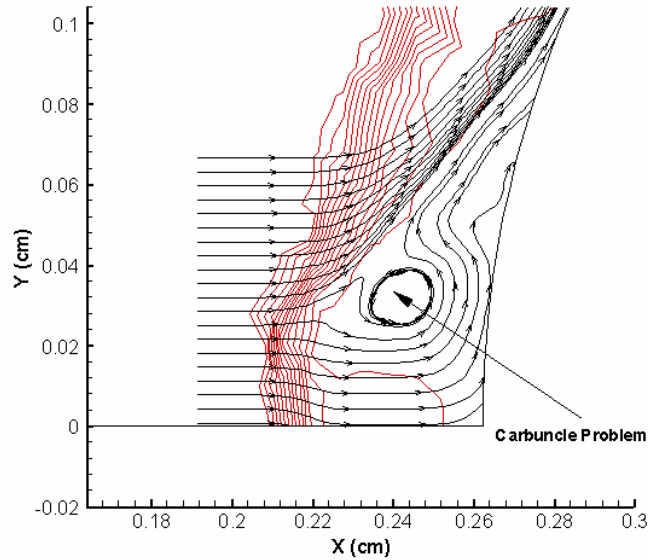


Figure 1. Velocity vectors showing carbuncle development.

This instability forms soon a protuberance in the region of nose. Starting simulations, a very small spurious vortex is still visible closest to the stagnation point. Since the magnitude of vorticity produced by a shock depends largely on the magnitude of the tangential velocity component, one will expect vortex severity to increase with increasing levels of velocity generated inside the structure of captured shock waves (Johnston, 1999). More artificial dissipation can avoid this carbuncle instability.

The Figure (2) presents the pressure contours obtained with 2<sup>nd</sup>-order Liou scheme, considering  $M_\infty = 12$ . The contours indicate that the flow are well captured by this solution, the bow shock and the flow expansion over the body are well represented. The shock at the nose of the body is a normal shock, and away from this the shock gradually becomes curved and weaker. The hypersonic flow ahead the normal shock becomes subsonic. Slightly above the nose region, the shock is oblique and pertains to the strong shock-wave solution. From the nose region until this point the flow is subsonic, and above it, all points on the shock correspond to the weak shock solution, and the region is characterized by supersonic flow.

The Figure (3) shows the temperature contours.

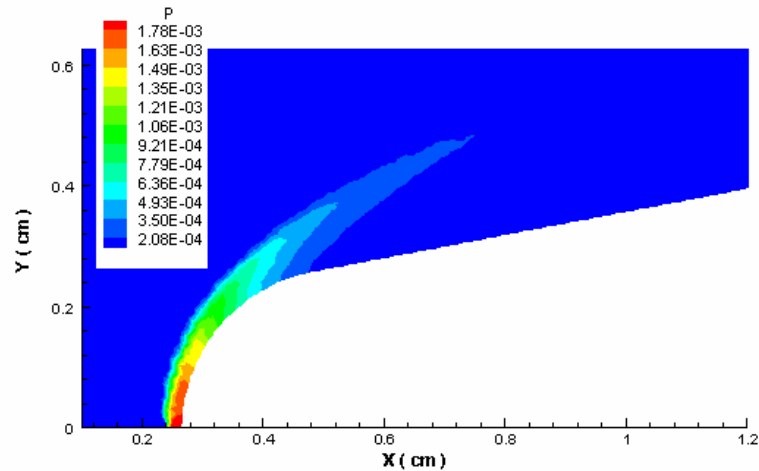


Figure 2. Pressure contours obtained considering  $M_\infty = 12$ .

One can observe that the temperature contours are well captured by this numerical method. The streamline that passes through this normal portion of the shock impinges on the nose of the body and controls the values of stagnation pressure and temperature at the nose.

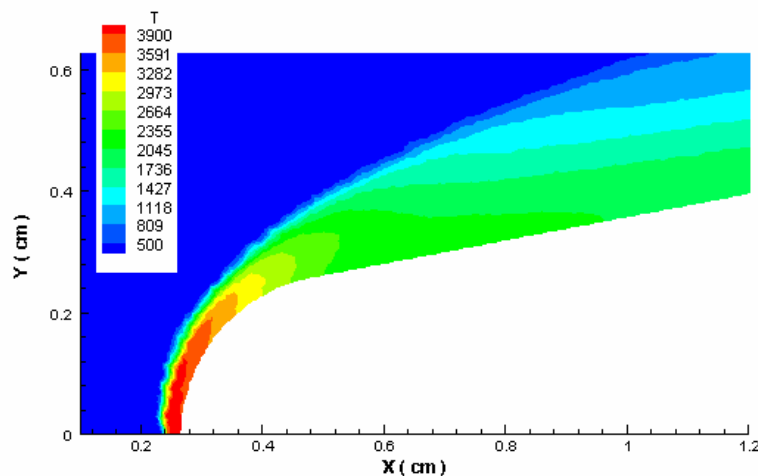


Figure 3. Temperature contours obtained considering  $M_\infty = 12$ .

## 5. Conclusions

The present work performed an inviscid hypersonic flow simulations over a small ballistic re-entry vehicle SARA configuration. For the numerical simulations real gas effects are incorporate into the solver. The governing equations are discretized in a cell centered finite volume algorithm. Unstructured meshes was used to obtain the numerical simulations. The equations are advanced in time by an explicit, 5-stage, 2<sup>nd</sup>-order accurate, Runge-Kutta time stepping procedure. The spatial discretization scheme considered a 2<sup>nd</sup>-order Liu flux-vector splitting scheme. A MUSCL reconstruction of primitive variable extrapolation was performed in order to obtain left and right states at interfaces. The results indicated that the scheme was able to reproduce some phenomena presented in hypersonic flow.

## 6. Acknowledgments

The authors wish to thank the Fundação de Amparo à Pesquisa do Estado de São Paulo (FAPESP, Brazil) for financial supporting.

## 7. References

- Anderson, Jr., J.D., "Hypersonic and High Temperature Gas Dynamics", McGraw-Hill, Inc., pp. 265-266, 1989.
- Azevedo, J.L.F., Korzenowski, H., "Comparison of Unstructured Grid Finite Volume Methods for Cold Gas Hypersonic Flow Simulation", 16th AIAA Applied Aerodynamics Conference, Jun. 98, Albuquerque, New Mexico, USA.
- Hachemin, Jean-Victor, 1995, "Development d'un code Navier-Stokes parabolise pour des ecoulements tridimensionnels en desequilibre thermochimique", Note Technique 1995-8, FR ISSN 0078-3781, France.
- Hirsh, C., Numerical Computation of Internal and External Flows. Vol. 2: Computational Methods for Inviscid and Viscous Flows, Wiley, New York, 1990.
- Johnston, I.A., 1999, "Simulation of Flow Around Hypersonic Blunt-Nosed Vehicles for the Calibration of Air Data Systems", Thesis of Doctor of Philosophy, University of Queensland,
- Kee, J.R., Rupley, F.M., Miller, J.A., 1991, CHEMIN-II: A fortran chemical kinetics package for the analysis of gas phase chemical kinetics, Sandia National Laboratories Technical Rep. SAND86-8009B/UC-706.
- Liou, M.-S., "A Sequel to AUSM: AUSM+", Journal of Computational Physics, vol. 129, 1996, pp. 374-382.
- Pimentel, C. A. R., Etude Numerique de La Transition entre Une Onde de Choc Oblique Stabilisee Par Un Diedre et Une Onde de Detonation Oblique, Thèse Doctorale, Université de Poitiers, 2000.